Contrasting Controls on the Phosphorus Concentration of Suspended Particulate Matter under Baseflow and Storm Event Conditions in Agricultural Headwater Streams

Richard J. Cooper[1*], Barry G. Rawlins[2], Tobias Krueger[3], Bertrand Lézé[1], Kevin M. Hiscock[1], Nikolai Pedentchouk[1]

[1]*School of Environmental Sciences, University of East Anglia, Norwich Research Park, Norwich, NR4 7TJ, UK*

[2] *British Geological Survey, Keyworth, Nottingham, NG12 5GG, UK*

[3] *IRI THESys, Humboldt University, 10099 Berlin, Germany*

*Correspondence: Richard.J.Cooper@uea.ac.uk; +44 (0)1603 591346

Abstract

Whilst the processes involved in the cycling of dissolved phosphorus (P) in rivers have been extensively studied, less is known about the mechanisms controlling particulate P concentrations during small and large flows. This deficiency is addressed through an analysis of large numbers of suspended particulate matter (SPM) samples collected under baseflow ($n = 222$) and storm event ($n = 721$) conditions over a 23-month period across three agricultural headwater catchments of the River Wensum, UK. Relationships between clay mineral and metal oxyhydroxide associated elements were assessed and multiple linear regression models for the prediction of SPM P concentration under baseflow and storm event conditions were formulated. These models, which explained 71-96% of the variation in SPM P concentration, revealed a pronounced shift in P association from iron (Fe) dominated during baseflow conditions to particulate organic carbon (POC) dominated during storm events. It is hypothesised this pronounced transition in P control mechanism, which is consistent across the three study catchments, is driven by changes in SPM source area under differing hydrological conditions. In particular, changes in SPM Fe-P ratios between small and large flows suggest there are three distinct sources of SPM Fe – surface soils, subsurface sediments and streambed iron sulphide. Further examination of weekly baseflow data also revealed seasonality in the Fe-P and aluminium oxalate-dithionate (Al_{ox}-Al_{di}) ratios of SPM, indicating temporal variability in

28   sediment P sorption capacity. The results presented here significantly enhance our understanding of

29   SPM P associations with soil derived organic and inorganic fractions under different flow regimes and

30   has implications for the mitigation of P originating from different sources in agricultural catchments.

31   **Keywords:** Fluvial; Suspended sediment; Geochemistry; Nutrient; Organic; Arable; Seasonality

1. Introduction

33   Diffuse phosphorus (P) pollution is a key factor behind the development of eutrophic conditions in

34   agricultural catchments (Withers and Jarvie, 2008; Quinton *et al*., 2010). As a naturally limiting

35   nutrient of plant growth in aquatic environments, dissolved P (DP) enrichment fuels blooms of

36   phytoplankton, periphyton and neuro-toxin secreting cyanobacteria colonies, which can dramatically

37   lower species diversity and lead to a fundamental breakdown of ecosystem functioning (Smith *et al*.,

38   1999; Hilton *et al*., 2006). P is dominantly transported through rivers in particulate form, with

39   sediment-associated P variously estimated to account for up to 90% of total P (TP) load in rural UK

40   catchments (e.g. Walling *et al*., 1997; Bowes *et al*., 2003). However, there exists a dynamic

41   equilibrium between the quantity of labile P associated with mineral surfaces and the concentration of

42   DP in both soil solution (Hartikainen *et al*., 2010) and in stream water (Palmer-Felgate *et al*., 2009)

43   which is controlled by biogeochemical processes. Consequently, understanding the importance of

44   sediment biogeochemistry in controlling particulate P (PP) concentrations is essential if DP

45   enrichment is to be mitigated.

46   Previous research has shown that DP reacts strongly with iron (Fe) and aluminium (Al) oxyhydroxide

47   complexes in soils and stream sediments to form mineral-bearing PP phases. This occurs principally

48   through the adsorption of phosphate ions onto solid phase mineral surfaces (non-occluded-P),

49   followed by the subsequent absorption of phosphate ions into the mineral itself (occluded-P) (Walker

50   and Syers, 1976; House and Denison, 2002; Evans *et al*., 2004). The rate at which this sorption

51   process occurs is a function of the availability of potential P binding sites on particulate surfaces. This

52   in turn is determined by factors such as mineral surface ionisation, presence of organic matter (OM)

53   complexes and competition from other anions. Additionally, oxyhydroxides commonly bind to clay

2

54 mineral surfaces via ligand exchange thereby forming an indirect association between P and the clay

55 mineral component of soils and sediments (House and Warwick, 1999; Withers and Jarvie, 2008;

56 Palmer-Felgate *et al.*, 2009).

57 Although much is known about how these processes affect the instream cycling of P, less is known

58 about how the relationships between PP and other organic and geochemical constituents change

59 during small and large flow periods. This is important because previous research has demonstrated

60 evidence of strong clockwise hysteresis in concentrations of both suspended particulate matter (SPM)

61 and PP during storm events in agricultural headwater catchments (Stutter *et al.*, 2008), thereby

62 providing evidence of changing SPM P associations under varying flow conditions. Whilst studies by

63 Van der Perk *et al.* (2007) and Rawlins (2011) developed regression models to demonstrate the

64 importance of a range of elements (Al, Ca, Ce, Fe, K, Mn) and phases (Al/Fe oxyhydroxides, clay

65 minerals, OM) in determining the P concentration of streambed sediments under baseflow conditions,

66 neither study considered how these associations changed under differing flows. In fact, to our

67 knowledge, no previous study has examined the geochemical associations between SPM and its P

68 bearing phases under different hydrological conditions in agricultural headwater catchments. This

69 represents a significant deficiency because source apportionment studies have demonstrated that there

70 can be a significant change in the sources of SPM under differing flows, with subsurface inputs linked

71 to baseflow sediment supply and increased surface source contributions associated with precipitation

72 events (Cooper *et al.*, 2015). Therefore, if the sources of SPM change under different flow regimes,

73 one can hypothesise that the organic and geochemical relationships between SPM and its P

74 component may be similarly affected.

75 Therefore, the main objectives of this study were:

76   (i)   to compare and contrast SPM organo-mineral relationships under baseflow and storm event

77   conditions;

78   (ii)   to develop multiple linear regression models to identify the importance of various organic

79   and inorganic parameters in determining SPM P concentration under differing flow regimes;

80   (iii)   to explore evidence of seasonality in SPM P concentration, Fe-P ratios and Al/Fe oxalate-

81   dithionate ratios, and to consider what these temporal trends reveal about variability in the

82   sources of SPM P.

83   This study was conducted over a 23-month period in a tributary of the lowland River Wensum, UK,

84   and formed part of a wider investigation into the sources of fine grained SPM in this agricultural

85   catchment.

2. Methods

2.1 Study Location

88   This study focused on the 20 km^2 Blackwater sub-catchment of the River Wensum, Norfolk, UK

89   (Figure 1). This intensive arable headwater catchment is monitored as part of the River Wensum

90   Demonstration Test Catchment (DTC) project which aims to evaluate the extent to which on-farm

91   mitigation measures can cost-effectively reduce diffuse agricultural pollution whilst maintaining food

92   production capacity (Outram *et al*., 2014). The Blackwater sub-catchment is divided into six 'mini-

93   catchments' A to F for observational purposes. Each mini-catchment has a bankside kiosk at the outlet

94   monitoring a variety of water quality parameters (e.g. pH, turbidity, temperature, ammonium,

95   chlorophyll, dissolved oxygen, stage) at 30-min resolution. Each kiosk also encompasses an automatic

96   water sampler (Teledyne ISCO, Lincoln, NE) containing 24, 1L polypropylene bottles which were

97   activated during heavy precipitation events to sample stream water.

98   Here, we focused solely upon mini-catchments A (5.4 km^2), B (1.3 km^2) and E (7.12 km^2), where

99   mini-catchments A and B are nested within mini-catchment E. Situated 30-60 m above sea level with

100   gentle slopes (<0.5°), intensive arable land constitutes 89% of these three headwater catchments, with

101   8% grassland, 2% mixed woodland and 1% rural settlements. The bedrock is Cretaceous white chalk

102   at a depth of ~20 m. Overlaying this are superficial deposits of Mid-Pleistocene diamicton glacial tills,

103   principally chalky, flint-rich boulder clays of the Sheringham Cliffs (0.2-0.5 m depth) and Lowestoft

104   Formations (0.5-20 m depth), interspersed with layers of glaciofluvial and glaciolacustrine sands and

105   gravels. Superimposed on this are deposits of Late Pleistocene silty loess (cover loam) and Holocene-

106   age alluvium and river terrace material. The principal surface soil types are clay loam to sandy clay

107   loam to a depth of >0.2 m (Hiscock *et al.*, 1996; Lewis, 2011). A weather station at the outlet to mini-

108   catchment A recorded average precipitation totals of 808 mm y^{-1} and mean average annual

109   temperatures of 9.2°C during the April 2012-March 2014 monitoring period.

110   2.2 Suspended Particulate Matter Sampling

111   Between May 2012 and March 2014, 6 L stream water grab samples were collected at 1-2 week

112   intervals under baseflow conditions at the outlets to mini-catchments A, B and E, yielding 222

113   samples in total. During the same period, the bankside automatic water samplers were remotely

114   activated to capture a total of 721 1 L grab samples at 60- or 120-min resolution during 14 storm

115   events at the same locations (where events are characterised by >8 mm of precipitation). All samples

116   were collected at the same depth and location in the center of the channel to ensure consistency

117   between baseflow and storm event SPM. The stream water samples were returned to the laboratory

118   and vacuum filtered through Millipore quartz fibre filter (QFF) papers with a retention rating of

119   99.1% at 0.7 µm to extract particulate matter. Sufficient water was filtered to obtain ~25 mg of SPM

120   on each filter. The SPM-covered filters were subsequently oven dried at 105°C for 2 hrs and weighed

121   to determine sediment mass retention and instream SPM concentrations.

122   2.3 Sediment Source Area Sampling

123   Four sources potentially contributing sediment to the River Blackwater where identified across mini-

124   catchments A and B. These were arable topsoils, damaged road verges, stream channel banks and

125   subsurface agricultural field drains. Both topsoil and road verge materials were collected as <50 mm

126   surface scrapes from areas susceptible to erosion that had high connectivity with the stream channel

127   (e.g. field entrances, tramlines, narrow road sections). Thirty samples from each of these surface

128   sources were collect in both mini-catchments A and B. Channel bank sediments were sampled as

129   surface scrapes at depths of 10, 30 and 50 cm above the streambed along the full reach of the river as

130   this represented the most heavily eroded section of the banks. Thirty bank samples were collected

131 from each mini-catchment. Sediments from 148 agricultural field drains identified across the mini-

132 catchments were collected by bulking together grab samples taken over a 12-month period. In total,

133 30 drain samples were collected from mini-catchment A and 18 from mini-catchment B. In the

134 laboratory, all source area samples were sonicated in a water bath for 7 min and wet sieved to <63 µm

135 to ensure comparable particle sizes and geochemistry with SPM. Approximately 25 mg of these

136 sediments were then vacuum filtered onto QFF papers and oven dried at 105°C for 2 hrs. Further

137 details on this sediment source sampling can be found in Cooper *et al*. (2015).

138 2.4 Spectroscopic Analysis

139 The geochemistry of all SPM-covered filter papers was analysed directly by X-ray fluorescence

140 spectroscopy (XRFS) and diffuse reflectance infrared Fourier transform spectroscopy (DRIFTS)

141 following the procedures described by Cooper *et al*. (2014). The concentrations of 11 elements (Al,

142 Ca, Ce, Fe, K, Mg, Mn, Na, P, Si, Ti) and five organic and inorganic phases (POC, dithionate-

143 extractable Al (Al_{di}) and Fe (Fe_{di}), oxalate-extractable Al (Al_{ox}) and Fe (Fe_{ox})) were determined. Also

144 calculated were Fe-P ratios, which are a useful indicator of P buffering capacity, and Al/Fe oxalate-

145 dithionate ratios, which effectively quantify the proportion of reactive (amorphous) to less reactive

146 (crystalline) oxyhydroxide phases.

147 2.5 Statistical Analysis

148 To begin with, the relationships between all measured SPM properties were assessed via correlation

149 panel plots for both baseflow and storm event samples. Then, to obtain a more comprehensive

150 understanding of SPM P control mechanisms, a series of regression analyses were performed for the

151 prediction of P under baseflow and storm event conditions for each of the three sampling locations (A,

152 B and E) such that six analyses were conducted in total. We initially formulated linear mixed effects

153 (LME) models with a temporal random effects component expressed in minutes since the earliest

154 sample using an exponential autoregressive correlation structure and restricted maximum likelihood

155 (REML) to provide unbiased parameter estimates. The purpose of this was to account for

156 autocorrelation in the geochemical time-series data. However, the inclusion of this temporal

157   autocorrelation did not significantly improve the model fit, thus rendering the use of the LME

158   approach redundant. We therefore adopted a simpler multiple linear regression approach based on

159   ordinary least squares (OLS) which was performed in the R environment (R Development Core Team,

160   2014). Due to heteroscedasticity in the distribution of SPM P values (based on inspection of

161   predictand histograms) these regression analyses were undertaken on log transformed P

162   concentrations. Predictors for all six regression models were selected based on prior knowledge of

163   their associations with P and included:

164   (i)   Metal oxyhydroxides ($Al_{ox/di}$, $Fe_{ox/di}$) and elements associated with metal oxyhydroxides (Fe,

165   Al, Mn);

166   (ii)   Elements associated with clay minerals (K, Mg, Na);

167   (iii)   Calcium (Ca) based on the co-precipitation of P with calcite (House, 2003);

168   (iv)   Phases associated with organic material (POC);

169   (v)   Elements strongly associated with particle size (Ti, Si) (Rawlins *et al*., 2009);

170   (vi)   Cerium (Ce) based in its enrichment in P-bearing apatite minerals (Rawlins, 2011);

171   (vii)   Channel stage, because flow volumes influence both SPM transport capacity and its

172   provenance.

173   A backwards elimination selection procedure was adopted, whereby an initial model including all of

174   the aforementioned predictors was formulated and any statistically insignificant regressors ($p > 0.05$)

175   were then removed one by one until only significant predictors remained. Variance inflation factor

176   (VIF) values were also calculated for each predictor as a measure of multicollinearity. Any predictor

177   with VIF values >10 were considered to have high multicollinearity and were therefore removed from

178   the model to minimise the risk of overfitting the regression. Once this final set of significant

179   predictors had been identified, the relative importance of each regressor was estimated and an

180   independent 10-fold cross-validation procedure was conducted to validate model results.

181   Lastly, time-series of SPM P concentration, Fe-P ratios and oxalate-dithionate ratios were plotted and

182   inspected for evidence of seasonality during the 23-month monitoring period. We used a 15 point,

7

183   second order Savitzky-Golay algorithm (Savitzky and Golay, 1964) to filter the time-series and

184   overlaid these on the plots to aid their interpretation.

3. Results and Discussion

3.1 Baseflow Geochemistry

187   Figure 2 presents the correlation plots for baseflow SPM geochemistry. Immediately apparent are the

188   very strong positive correlations between Al and Mg ($r = 0.95$), Al and K ($r = 0.92$) and Mg and K (r

189     $= 0.84$) which indicate the presence of clay minerals which contain significant amounts of all three

190   cations. Strong positive correlations also exist between Al and Ti ($r = 0.75$), K and Ti ($r = 0.77$) and

191   Na and Mg ($r = 0.72$), further supporting the presence of clay minerals within SPM, with 70% of

192   kaolinite minerals reported to contain Ti (Dolcater *et al*., 1970). Another notable association is that

193   between Fe and P ($r = 0.71$), which likely indicates P sorbing to the solid phase mineral surfaces of

194   Fe-containing compounds. However, somewhat unexpectedly, P is not correlated with the abundance

195   of either Fe_{di} or Fe_{ox}. This may in part be explained by the occurrence of range of poorly crystalline

196     $Fe^{(II)}$ or mixed $Fe^{(II)}/Fe^{(III)}$ minerals (alongside FeOOH) that have vastly different P binding properties,

197   as observed by Bortleson (1974) based on the analyses of lake sediments. The non-specific nature of

198   oxalate and diothionite extractions likely results in the dissolution of amorphous and crystalline forms

199   of Fe with a wide range of P sorption capacities resulting in a weak overall correlation with total P.

200   There is also no obvious association between P and Ce ($r = 0.19$), in contrast to the findings of

201   Rawlins (2011) who demonstrated that variations in Ce could explain 10.4% of the variability in bed

202   sediment P concentration in rivers across central England.

203   With respect to the organic fraction, POC exhibits negligible correlation with SPM P ($r = 0.06$) under

204   baseflow conditions, suggesting a dominantly inorganic control on baseflow SPM P concentrations.

205   Instead, POC correlates most strongly with Fe_{ox} ($r = 0.66$), which may be explained by (i) the sorption

206   of POC onto the surfaces of Fe oxyhydroxides which, due to their large specific surface areas,

207   commonly have sorption rates an order of magnitude greater than many common clay minerals; or (ii)

208   the stabilisation and protection from degradation afforded to POC through the formation of organo-Fe

209   complexes (Kaiser and Guggenberger, 2003; Wagai and Mayer, 2007). Furthermore, it has been

210   demonstrated that the amorphous Fe compounds tend to be more important than crystalline

211   oxyhydroxides in this stabilisation process (Wilson *et al*., 2013). Evidence for this can be seen here,

212   with stronger linear correlations between POC and the amorphous Fe_{ox} ($r = 0.66$) than with crystalline

213   Fe_{di} ($r = 0.15$).

3.2 Storm Event Geochemistry

215   Figure 3 presents the correlation plots for storm event SPM geochemistry. Strong, positive

216   correlations are again apparent between Al and K ($r = 0.93$), Al and Mg ($r = 0.89$) and K and Mg ($r =$

217   0.87), once more indicating that clay mineral composition likely dominates these geochemical

218   associations. Strong correlations between Al and Ti ($r = 0.82$), K and Ti ($r = 0.84$) and Mg and Ti ($r =$

219   0.79), indicate Ti oxides in association with these clay minerals. Compared with baseflow conditions,

220   linear correlations between Ce and K ($r = 0.85$), Ce and Al ($r = 0.82$) and Ce and Ti ($r = 0.78$) are

221   substantially stronger, which may reflect an increased supply of SPM from Ce enriched topsoil and

222   road verge sediments during heavy precipitation events (Cooper *et al*., 2015).

223   Importantly, P exhibits a strong positive correlation with POC during storm events ($r = 0.56$), in

224   contrast to its association under baseflow conditions. This relationship is consistent with similar

225   findings by Walling *et al*. (2001) for four other UK rivers (Seven, Avon, Exe and Dart) under storm

226   event flows. POC also correlates strongly with Mn ($r = 0.69$), as does P ($r = 0.51$). Previous research

227   has demonstrated that Mn can be particularly effective in the sorption of P, with freshly precipitated

228   Mn hydroxides (which likely form in streambed sediments under varying redox conditions) found to

229   have a higher P sorption capacities than equivalent Fe or Al hydroxides (Lu and Liao, 1997).

230   However, Lu and Liao (1997) also showed that on ageing Mn became the least effective of the three

231   metals in terms of sorption capacity.

3.3 Determining SPM P Control Mechanisms

3.3.1 Baseflow Regression Models

234   The baseflow multiple regression models (Table 2) explain 76-96% of the variance in SPM P

235   concentrations at each of the three sites based on between four and six geochemical predictors.

236   Variation in total Fe concentration is a consistently dominant predictor, explaining 37%, 12% and

237   38% of SPM P variability at sites A, B and E, respectively. The sorption of P onto the surfaces of Fe

238   containing complexes represents the most likely causal mechanism for this strong, positive Fe-P

239   association. Similarly, sorption of P onto the surfaces of metal oxyhydroxides would explain the

240   significant association with Al_{ox} at site A ($R^2 = 0.156$) and with Mg at site A ($R^2 = 0.049$) and site E

241   ($R^2 = 0.112$). Interestingly, neither K nor Na are significant predictors, suggesting that the quantity or

242   type of clay minerals in SPM is not a dominant control of baseflow SPM P in these catchments.

243   A strong negative relationship with Ti is observed at site A ($R^2 = 0.224$) and site E ($R^2 = 0.449$),

244   although it is not a significant predictor at site B. The most likely host for Ti is secondary Ti oxides,

245   which tend to be fine-grained and form associations with other mineral phases. If the Ti in SPM is a

246   secondary oxide, its strong linear correlations with Al, K and Mg ($r > 0.66$; Figure 2) suggest it is

247   closely associated with certain clay minerals which are less enriched in P than Fe containing phases,

248   hence the negative association. At site B, Si is the dominant predictor of SPM P ($R^2 = 0.445$), with

249   this strong, positive association contrasting strongly with the regression results for sites A and E. High

250   SPM Si concentrations typically indicate an abundance of coarse quartz material and thus a strong

251   positive association with P, which tends to be enriched in fine sediment, would not intuitively be

252   expected. However, Si is strongly and negatively associated with Ti ($r = -0.60$; Figure 2) and thus the

253   association between P and Si at site B may reflect collinearity between these two predictors.

254   POC is a relatively weak predictor under baseflow conditions, explaining just 1% of the variance in

255   SPM P concentrations at site A and 8% at sites B and E. Similarly, Ce was a weak predictor at site B

256   ($R^2 = 0.062$), whilst Ca was insignificant at all sites implying that abiotically mediated co-

257   precipitation of P with calcite is not an important control of SPM P concentrations. Overall, these

258   multiple regression model results indicate that the abiotic sorption of P onto the surfaces of Fe

259   containing complexes is a dominant control of baseflow SPM P concentrations in the River

260   Blackwater.

3.3.2 Storm Event Regression Models

The storm event regression models explain 71-94% of the variance in SPM P concentrations across the three sites based on between four and eight predictors (Table 3). Importantly, the results reveal a clear shift in P association, from Fe-dominated under baseflow conditions to POC-dominated during storm events. Variability in POC concentrations are able explain 21%, 62% and 20% of the variance in SPM P at sites A, B and E, respectively, making it the strongest predictor at two of these locations. This P-POC association may relate to OM being a source of P through mineralization reactions and soluble reactive phosphorus (SRP) sorbing onto the surfaces of OM in soils and sediments. However, organic molecules also liberate phosphate ions into solution by replacing them on clay mineral and metal oxyhydroxide surface binding sites, whilst also blocking the pore spaces of mineral aggregates and acting as a protective barrier around mineral surfaces (Kaiser and Guggenberger, 2003; Wagai *et al.*, 2013). Despite these opposing processes, numerous studies have commented upon the link between P and OM in stream sediments, with most establishing similar positive associations to that observed here (e.g. Rawlins, 2011; Krueger *et al.*, 2012).

In further contrast to the baseflow regression models, Mn is a strong and significant predictor of P during storm events at site A ($R^2 = 0.275$) and site E ($R^2 = 0.165$). This likely reflects both Mn association with POC ($r = 0.69$; Figure 3) and the sorption of P onto the surfaces of metal oxides. Channel stage is also a strong and significant predictor at site A ($R^2 = 0.182$), indicating a dilution of SPM P concentrations under larger flows. Despite its much reduced importance, Fe remains a significant predictor of P during storm events at site A ($R^2 = 0.101$) and site E ($R^2 = 0.055$), confirming the sorption of P onto Fe containing complexes. Significant associations are again evident with Ti at sites A ($R^2 = 0.043$) and E ($R^2 = 0.150$), and with Si at sites B ($R^2 = 0.038$) and E ($R^2 = 0.174$), but these regressors are generally weaker predictors than that observed in the baseflow models. Overall, these multiple regression models indicate that storm event SPM P concentrations are dominantly associated with organic matter complexes.

3.3.3 Interpreting Regression Results

287 The pronounced transition from Fe-P dominated associations under baseflow conditions to POC-P

288 associations during storm events can most likely be explained by a change in SPM source area.

289 Previous sediment fingerprinting research in the same catchment (Cooper *et al.*, 2015) demonstrated

290 baseflow SPM source contributions are dominated by subsurface inputs (i.e. stream channel banks and

291 agricultural field drains) which have significantly (*t*-test $p<0.01$) larger Fe-POC ratios compared with

292 surface sources (i.e. road verge material and arable topsoils) (Table 1). This creates geochemical

293 conditions conducive to the sorption of phosphate ions onto the surfaces of Fe containing complexes,

294 hence the dominance of the Fe-P association during baseflow. This association may arise in either the

295 stream, soil or field drains as a consequence of changing redox conditions initiating the precipitation

296 of Fe bound P (Jarvie *et al.*, 2008). Conversely, during storm events, SPM was demonstrated to

297 comprise a greater contribution from surface sources which have significantly (*t*-test $p<0.01$) smaller

298 Fe-POC ratios (Table 1). This results in larger quantities of P being either transported with, or sorbed

299 onto the surfaces of, OM-bearing complexes, hence the greater importance of the P-POC association

300 observed in the storm event regression models.

301 The data also indicate that another distinct source of Fe-enriched SPM is mobilized during storm

302 events. Evidence for this comes from examining the SPM Fe-P ratios which increase during large

303 storm events relative to baseflow conditions (Figure 4). Because surface soils have substantially lower

304 Fe-P ratios than subsurface sediments (Table 1), we hypothesize this increase in the Fe-P ratio of SPM

305 is caused by storm event mobilization of iron sulphide (FeS) which commonly forms in the reducing

306 conditions beneath the surface of streambeds (Large et al., 2001). A coupled scanning electron

307 microscopy and energy dispersive X-ray spectroscopy (SEM-EDS) analysis of sediments collected

308 from the surface of the streambed (0-6 cm depth) at site E confirmed the presence of iron sulphides

309 within the easily mobilised fine (<63 µm) sediment fraction, thus supporting this hypothesis (Figure

310 5).

311 **3.4 Temporal Trends in Baseflow SPM Composition**

312 *3.4.1 Phosphorus*

313   Figure 6 presents the time-series of SPM P concentrations under baseflow conditions at 1-2 week

314   intervals between May 2012 and March 2014. Whilst no consistent temporal trend is recorded across

315   the three sites, a very strong seasonal cycle is recorded at site E with concentrations larger during the

316   summer/autumn and smaller during the winter/spring. The timings of these peaks may be linked to a

317   combination of (i) increased autochthonous P release as a consequence of growing season primary

318   production; (ii) the development of P-rich biofilms around fine particulates which grow more

319   vigorously during the summer; (iii) enhanced bed sediment P sorption under low flows; or (iv)

320   increased P-rich SPM inputs from subsurface field drains. These summer/autumn P peaks correspond

321   with similar findings for a range of other UK rivers under differing hydrological conditions (Walling

322   *et al*., 2001, Stutter *et al*., 2008, Ballantine *et al*., 2009).

323   Conversely, SPM P concentrations at site B exhibited three local minima in August 2012, July 2013

324   and January 2014 and a global maximum in April 2013, whilst concentrations at site A were small

325   and stable between May 2012 and April 2013 before rising sharply during summer 2013. Previous

326   studies have linked such spatial intra-catchment variability in P concentrations to differences in

327   geology, land-use and point sources of pollution such as sewage treatment works (e.g. Ballantine *et*

328   *al*., 2008). However, considering the short distance between sites A, B and E (600 m) and the absence

329   of any sewage discharges between them, we can rule these out as explanatory factors. Instead, these

330   spatial differences in SPM P concentration likely relate to localised instream primary production and

331   inputs from agricultural field drains which have previously been shown to be important pathways for

332   SPM in this catchment (Cooper *et al*., 2015) and may transport SRP from agricultural fertilizers

333   directly into the stream channel. It is also worth noting that summer 2013 was warmer (mean monthly

334   temperature 0.5°C higher) and drier (mean monthly precipitation 45 mm lower) than summer 2012,

335   conditions conducive to vigorous instream primary productivity which may partly explain the higher

336   P peaks observed at all sites during 2013.

337   *3.4.2 Iron-Phosphorous Ratios*

338   Previous research has demonstrated that Fe-P ratios can be useful indicators of the P buffering

339   capacity of aquatic sediments (Jensen *et al.*, 1992). Specifically, the higher the Fe-P ratio, the greater

340   the potential for the adsorption of SRP onto the surfaces of Fe containing compounds within

341   sediments. Thus, higher Fe-P ratios allow sediment to isolate SRP from uptake by biota and thereby

342   minimize the risk of eutrophication.

343   In the River Blackwater, baseflow SPM Fe-P ratios during winter/spring 2012 were approximately

344   double that recording during the following summer/autumn, particularly at sites A and E (Figure 6).

345   This implies SPM had greater capacity to adsorb excess SRP outside of the growing season. Strong,

346   negative linear correlations between the Fe-P ratio and SPM P at sites A (r = -0.78), B (r = -0.56) and

347   E (r = -0.84) indicate variation in SPM P concentration, and not SPM Fe, was the main driver behind

348   variability in these ratios. This could be explained by greater autochthonous P production during the

349   summer leading to greater P sorption onto Fe-bearing sediments which lowered the Fe-P ratios during

350   the summer months. For all sites, ratios observed across the seasons were within the range of values

351   (1-290) reported by House and Denison (2002) for six British rivers and generally greater than 15, the

352   value above which it has been shown sediments can moderate temporal SRP variability in lacustrine

353   environments (Jensen *et al.*, 1992).

354   *3.4.3 Oxalate-Dithionate Ratios*

355   The ratio of oxalate-extractable (amorphous) to dithionate-extractable (crystalline) Fe and Al can be

356   used as an index of the P sorption capacity of SPM. The time-series presented in Figure 7 reveal a

357   clear seasonal cycle in the Al_{ox}-Al_{di} ratios at all sites, with a greater proportion of reactive amorphous

358   material present during the summer months and less during the winter. This cycle is primarily driven

359   by variation in the amorphous Al_{ox} fraction, which correlates strongly and positively with the Al_{ox}-

360   Al_{di} ratios at sites A (r = 0.78), B (r = 0.53) and E (r = 0.57). In contrast with the Fe-P ratios, these

361   Al_{ox}-Al_{di} ratios imply that SPM during the biologically sensitive summer season had a higher P

362   adsorption capacity and thus greater ability to capture and transport SRP through the stream network.

363   This conclusion is supported by the correlation between P and Al_{ox} under baseflow conditions (r =

0.49), which was the strongest association of the four Fe and Al oxyhydroxide compounds, and second only to total Fe ($r = 0.71$) for overall correlation with SPM P (Figure 2).

Based on the composition of sediment source areas (Table 1), we can hypothesise that field drains with enriched Al_{ox}-Al_{di} ratios supplied a greater proportion of Al_{ox} during the summer, whilst contributions from channel banks and road verges with lower Al_{ox}-Al_{di} ratios were more significant during the winter. Therefore, the SPM discharged by agricultural field drains appears to play an important role in determining the transport of SPM P during the growing season when streams are more sensitive to the detrimental effects of eutrophication. However, other processes may also be contributing to the higher proportion of Al_{ox} observed during the summer months. For example, Violante and Violante (1980) demonstrated that higher concentrations of organic ligands slow down the crystallisation of Al oxyhydroxides (i.e. the formation of Al_{di}). During the growing season, plants release larger quantities of organic acids into soil solution which would restrict the formation of Al_{di} and thus increase the proportion of Al_{ox}, thereby accounting for the higher Al_{ox}-Al_{di} ratios observed in SPM during this period.

Interestingly, both the magnitude and timing of maxima and minima in Al_{ox}-Al_{di} ratios are different between years, with the winter 2012/13 minima occurring ~2 months earlier and being considerably more pronounced than during the corresponding winter 2013/14, for example. This can be explained by a combination of higher rainfall totals and different crop cultivation practices during autumn 2012 altering the sources of SPM compared with the following year.

Seasonality in the Fe_{ox}-Fe_{di} ratios is much less apparent than that observed for Al_{ox}-Al_{di} (Figure 7) and based on the overall weakness of these trends we cannot make any conclusive statements regarding seasonality in these ratios.

3.5 Significance and Further Research

Through our analysis of large numbers of SPM samples collected under small and large flows at three adjacent agricultural catchment locations, we present clear evidence of a pronounced change in SPM P control mechanisms; from Fe-dominated associations under baseflow conditions, to POC-dominated

390 associations during storm events. Because the most likely cause of this change is a shift in SPM

391 source area under different hydrological conditions, this is likely to be a widespread phenomenon.

392 This finding has implications for mitigation measures aimed at reducing fluvial SPM P transfers in

393 agricultural catchments, suggesting that different sediment source areas need to be targeted to reduce

394 P contributions under differing hydrological conditions. This could include the installation of roadside

395 sediment traps to capture P-rich particulates in surface runoff during storm events (Cooper *et al*.,

396 2015), or the employment of minimum cultivation techniques to minimize preferential flows of

397 nutrients through subsurface drainage networks under baseflow conditions (Stevens and Quinton,

398 2009).

399 Furthermore, to our knowledge, this is the first study to demonstrate distinct seasonality in SPM Al_{ox}-

400 Al_{di} ratios in an agricultural headwater catchment. This observation has important implications for (i)

401 understanding the extent of P availability for exchange between dissolved and particulate forms and

402 (ii) for the development of eutrophic conditions during the ecologically sensitive summer period. The

403 European wide study by Hartikainen *et al*. (2010) showed that both equilibrium P concentration (the

404 'zero point' of P exchange at which no net desorption from, or sorption to, sediment occurs) and the

405 quantity of instantly labile P were strongly correlated with the P saturation degree of Al

406 oxyhydroxides. The larger surface area and associated exchange capacity of amorphous, compared to

407 crystalline, Al oxyhydroxides will likely alter their degree of P saturation (Bohn *et al*., 1979). The

408 degree of P saturation of Al oxyhydroxides may differ between summer and winter due to the

409 differences in the proportions of amorphous and crystalline phases we observed in each of the three

410 streams we studied, so comparisons between P saturation of Al oxyhydroxides in suspended and bed

411 sediments of other headwater channels during winter and summer warrants further investigation.

412 Lastly, the enriched Al_{ox}-Al_{di} ratios of SPM derived from agricultural field drains indicates that these

413 subsurface drainage networks, which are widespread throughout the intensive arable systems of

414 Europe and North America, are potentially important for controlling the instream concentration of

415 reactive P. Consequently, mitigation measures aimed at reducing SPM discharges from field drains

416 could decrease the amount of Al_{ox} associated P in agricultural headwater streams.

4. Conclusions

In this study, we have used large numbers of SPM samples collected under baseflow ($n = 222$) and storm event ($n = 721$) conditions to demonstrate contrasting control mechanisms on SPM P concentration under different flow regimes in three lowland agricultural headwater catchments. Multiple linear regression models reveal a pronounced shift in P association, from Fe-dominated under baseflow conditions to POC-dominated during storm events. It is hypothesised that this transition in P control mechanism, which is spatially consistent across the three study catchments, is driven by changes in the dominant SPM source area. Specifically, greater SPM supply is thought to originate from subsurface stream channel banks and agricultural field drains with comparatively high Fe-POC ratios during baseflow conditions, coupled with increased autochthonous P contributions. Conversely, contributions from surface soils with comparatively depleted Fe-POC ratios are thought to increase during storm events, along with the erosive mobilization of iron sulphide from beneath the surface of the streambed. Further examination of weekly baseflow data revealed evidence of seasonality in both Fe-P and Al oxalate-dithionate (Al_{ox}-Al_{di}) ratios over a 23-month period. This indicates temporal variability in the P sorption capacity of SPM and is also thought to relate to changes in SPM source area. The results presented here significantly enhance our understanding of the contrasting control mechanisms of SPM P under varying flow regimes and have important implications for the targeting of P mitigation measures in agricultural catchments under different hydrological conditions.

Acknowledgements

443 version of this manuscript. This paper is published with the permission of the Executive Director of
444 the British Geological Survey (Natural Environment Research Council).

445 **References**

446 Ballantine, D.J., Walling, D.E., Collins, A.L., Leeks, G.J.L., 2008. The phosphorus content of fluvial
447   suspended sediment in three lowland groundwater-dominated catchments. Journal of
448   Hydrology 357, 140-151. DOI: 10.1016/j.jhydrol.2008.05.011.

449 Ballantine, D.J., Walling, D.E., Collins, A.L., Leeks, G.J.L., 2009. The content and storage of
450   phosphorus in fine-grained channel bed sediment in contrasting lowland agricultural
451   catchments in the UK. Geoderma 151, 141-149. DOI: 10.1016/j.geoderma.2009.03.021.

452 Bohn, H.L., McNeal, B.L., O'Connor, G.A., 1979. Soil chemistry. John Wiley & Sons, New York.

453 Bortleson, G.C., 1974. Phosphorus, iron and manganese distribution in sediment cores of six
454   Winconsin lakes. Limnology and Oceanography 19, 794-801.

455 Bowes, M.J., House, W.A., Hodgkinson, R.A., 2003. Phosphorus dynamics along a river continuum.
456   Science of the Total Environment 313, 119–212. DOI: 10.1016/S0048-9697(03)00260-2.

457 Cooper, R.J., Rawlins, B.G., Lézé, B., Krueger, T., Hiscock, K., 2014. Combining two filter paper-
458   based analytical methods to monitor temporal variations in the geochemical properties of
459   fluvial suspended particulate matter. Hydrological Processes 28, 4042-4056. DOI:
460   10.1002/hyp.9945.

461 Cooper, R.J., Krueger, T., Hiscock, K.M., Rawlins, B.G., 2015. High-temporal resolution fluvial
462   sediment source fingerprinting with uncertainty: a Bayesian approach. Earth Surface
463   Processes and Landforms 40, 78-92. DOI: 10.1002/esp.3621.

464 Dolcater, D.L., Syers, J.K., Jackson, M.L., 1970. Titanium as free oxide and substituted forms in
465   kaolinites and other soil minerals. Clays and Clay Minerals 18, 71-79.

466 Evans, D.J., Johnes, P.J., Lawrence, D.S., 2004. Physico-chemical controls on phosphorus cycling in
467   two lowland streams. Part 2 – The sediment phase. Science of the Total Environment 329,
468   165-182. DOI: 10.1016/j.scitotenv.2004.02.023.

469 Hartikainen, H., Rasa, K., Withers, P.J.A., 2010. Phosphorus exchange properties of European soils
470   and sediments derived from them. European Journal of Soil Science 6, 1033-1042. DOI:
471   10.1111/j.1365-2389.2010.01295.x.

472 Hilton, J., O'Hare, M., Bowes, M.J., Jones, J.I., 2006. How green is my river? A new paradigm of
473   eutrophication in rivers. Science of the Total Environment 365, 66-83.
474   DOI:10.1016/j.scitotenv.2006.02.055.

475 Hiscock, K.M., Dennis, P.F., Saynor, P.R., Thomas, M.O., 1996. Hydrochemical and stable isotope
476   evidence for the extent and nature of the effective Chalk aquifer of north Norfolk, UK.
477   Journal of Hydrology 180, 79-107. DOI: 10.1016/0022-1694(95)02895-1.

478 House, W.A., Warwick, M.S., 1999. Interactions of phosphorus with sediments in the River Swale,
479   Yorkshire, UK. Hydrological Processes 13, 1103-1115.

480

481 House, W.A., Denison, F.H., 2002. Total phosphorus content of river sediments in relationship to
482   calcium, iron and organic matter concentrations. Science of the Total Environment 282-283,
483   341-351. DOI: 10.1016/S0048-9697(01)00923-8.

484 House, W.A., 2003. Geochemical cycling of phosphorus in rivers. Applied Geochemistry 18, 739-
485   748. DOI: 10.1016/S0883-2927(02)00158-0.

486 Jarvie, H.P., Haygarth, P.M., Neal, C., Butler, P., Smith, B., Naden, P.S., Joynes, A., Neal, M.,
487   Wickham, H., Armstrong, L., Harman, S., Palmer-Felgate, E.J., 2008. Stream water chemistry
488   and quality along an upland-lowland rural land-use continuum, south west England. Journal
489   of Hydrology 350, 215-231. DOI: 10.1016/j.jhydrol.2007.10.040.

490   Jensen, H.S., Kristensen, P., Jeppesen, E., Skytthe, A., 1992. Iron:phosphorus ratio in surface

491   sediments as an indicator of phosphate release from aerobic sediments in shallow lakes.

492   Hydrobiologia 235-236, 731-743.

493   Kaiser, K., Guggenberger, G., 2003. Mineral surfaces and soil organic matter. European Journal of

494   Soil Science 54, 219-236. DOI: 10.1046/j.1365-2389.2003.00544.x.

495   Krueger, T., Quinton, J.N., Freer, J., Macleod, C.J.A., Bilotta, G.S., Brazier, R.E., Hawkins, J.M.B.,

496   Haygarth, P.M., 2012. Comparing empirical models for sediment and phosphorus transfer

497   from soils to water at field and catchment scale under data uncertainty. European Journal of

498   Soil Science 63, 211-223. DOI: 10.1111/j.1365-2389.2011.01419.x.

499   Large, D.J., Fortey N.J., Milodowski, A.E., Christy, A.G., Dodd, J., 2001. Petrographic observations

500   of iron, copper, and zinc sulphides in freshwater canal sediment. Journal of Sedimentary

501   Research 71, 61-69. DOI: 10.1306/052600710061.

502   Lewis, M.A., 2011. Borehole drilling and sampling in the Wensum Demonstration Test Catchment.

503   British Geological Survey Commissioned Report, CR/11/162. 38pp, National Environment

504   Research Council, Keyworth, Nottingham, UK.

505   Lu, Q., Liao, Z., 1997. Comparative study on characteristics of P fixation by Mn, Fe and Al.

506   Pedosphere, 7, 325-330.

507   Outram, F.N., Lloyd, C.E.M., Jonczyk, J., Benskin, C.M.H., Grant, F., Perks, M.T., Deasy, C., Burke,

508   S.P., Collins, A.L., Freer, J., Haygarth, P.M., Hiscock, K.M., Johnes, P.J., Lovett, A.L., 2014.

509   High-frequency monitoring of nitrogen and phosphorus response in three rural catchments to

510   the end of the 2011-2012 drought in England. Hydrology and Earth System Sciences 18,

511   3429-3448. DOI: 10.5194/hess-18-3429-2014.

512   Palmer-Felgate, E.J., Jarvie, H.P., Withers, P.J.A., Mortimer, R.J.G., Krom, M.D., 2009. Stream-bed

513   phosphorus in paired catchments with different agricultural land use intensity. Agriculture,

514   Ecosystems and Environment 134, 53-66. DOI:10.1016/j.agee.2009.05.014.

515   Quinton, J.N., Govers, G., Oost, K.V., Bardgett, R.D., 2010. The impact of agricultural soil erosion on

516   biogeochemical cycling. Nature Geoscience 3, 311-314. DOI: 10.1038/NGEO838.

517   R Development Core Team, 2014. R: A language and environment for statistical computing. R

518   Foundation for Statistical Computing: Vienna, Austria. http://www.R-project.org.

519   Rawlins, B.G., Webster, R., Tye, A.M., Lawley, R., O'Hara, S.L., 2009. Estimating particle-size

520   fractions of soil dominated by silicate minerals from geochemistry. European Journal of Soil

521   Science 60, 116-126. DOI: 10.1111/j.1365-2389.2008.01112.x.

522   Rawlins, B.G., 2011. Controls on the phosphorus content of fine stream bed sediment in agricultural

523   headwater catchments at the landscape scale. Agriculture, Ecosystems and Environment 144,

524   352-363. DOI: 10.1016/j.agee.2011.10.002.

525   .

526   Savitzky, A., Golay, M.J., 1964. Smoothing and differentiation of data by simplified least square

527   procedures. Analytical Chemistry 36, 1627–1639. DOI: 10.1021/ac60214a047.

528   Smith, V.H., Tilman, G.D., Nekola, J.C., 1999. Eutrophication: impacts of excess nutrient inputs on

529   freshwater, marine, and terrestrial ecosystems. Environmental Pollution 100, 179-196.

530   DOI:10.1016/S0269-7491(99)00091-3.

531   Stevens, C., Quinton, J. 2009. Diffuse pollution swapping in arable agricultural systems. Critical

532   Reviews   in   Environmental   Science   and   Technology   39,   478-520.   DOI:

533   10.1080/10643380801910017

534   Stutter, M.I., Langan, S.J., Cooper, R.J., 2008. Spatial and temporal dynamics of stream water

535   particulate and dissolved N, P and C forms along a catchment transect, NE Scotland. Journal

536   of Hydrology 350, 187-202. DOI: 10.1016/j.jhydrol.2007.10.048.

537   Van der Perk, M., Owens, P.N., Deeks, L.K., Rawlins, B.G., Haygarth, P.M., Beven, K.J., 2007.

538   Controls on catchment-scale patterns of phosphorus in soil, streambed sediment, and stream

539   water. Journal of Environmental Quality 36, 694-708. DOI:10.2134/ jeq2006.0175.

540   Violante, A. Violante, P., 1980. Influence of pH, concentration, and chelating power of organic anions

541   on the synthesis of aluminium hydroxides and oxyhydroxides. Clay and Clay Minerals 28,

542   425-434.

543   Wagai, R., Mayer, L.M., 2007. Sorptive stabilization of organic matter in soils by hydrous iron

544   oxides. Geochimica et Cosmochimica Acta 71, 25:35. DOI: 10.1016/j.gca.2006.08.047.

545   Wagai, R., Mayer, L.M., Kitayama, K., Shirato, Y., 2013. Association of organic matter with iron and

546   aluminium across a range of soils determined via selective dissolution techniques coupled

547   with dissolved nitrogen analysis. Biogeochemistry 112, 95-109. DOI: 10.1007/s10533-011-

548   9652-5.

549   Walker, T.W., Syers, J.K., 1976. The fate of phosphorus during pedogenesis. Geoderma 15, 1-19.

550   DOI: 10.1016/0016-7061(76)90066-5.

551   Walling, D.E., Webb, B.W., Russell, M.A., 1997. Sediment-associated nutrient transport in UK rivers.

552   In: Webb, B. (Ed.) Freshwater Contamination. IAHS Publication, pp. 69–81.

553   Walling, D.E., Russell, M.A., Webb, B.W., 2001. Controls on the nutrient content of suspended

554   sediment transported by British rivers. Science of the Total Environment 266, 113-123. DOI:

555   10.1016/S0048-9697(00)00746-4.

556   Wilson, C.A., Cloy, J.M., Graham, M.C., Hamlet, L.E., 2013. A microanalytical study of iron,

557   aluminium and organic matter relationships in soils with contrasting hydrological regimes.

558   Geoderma 202-203, 71-81. DOI: 10.1016/j.geoderma.2013.03.020.

559   Withers, P.J.A, Jarvie, H.P., 2008. Delivery and cycling of phosphorus in rivers: A review. Science of

560   the Total Environment 400, 379-395. DOI: doi:10.1016/j.scitotenv.2008.08.002.

561

562

563

564

Figure Captions

Graphical Abstract: Conceptual diagram of the contrasting controls on SPM phosphorus

concentration in agricultural headwater streams under different hydrological conditions.

Figure 1: The Blackwater sub-catchment study area, showing land cover types in mini-catchments A,

B and E, with the wider River Wensum catchment also shown.

Figure 2: Correlation panel plot of SPM geochemistry (% by weight) under baseflow conditions at

sites A, B and E ($n = 222$). Stage is recorded in meters. The upper right section displays Pearson's

correlation coefficients with the text size proportional to correlation strength. The bottom left panel

shows the SPM samples (points) and linear regression (line). Central histograms show the distribution

of values for each parameter.

Figure 3: Correlation panel plot of SPM geochemistry (% by weight) under storm event conditions at

sites A, B and E ($n = 721$). Stage is recorded in meters. The upper right section displays Pearson's

correlation coefficients with the text size proportional to correlation strength. The bottom left panel

shows the SPM samples (points) and linear regression (line). Central histograms show the distribution

of values for each parameter.

Figure 4: Time-series of SPM Fe-P ratios for sites A, B and E during three consecutive storm events

in November 2012. Baseflow mean refers to the average for all three sites.

Figure 5: Evidence of iron sulphides revealed by an SEM-EDS analysis of sediment collected from

the streambed surface (0-6 cm depth) at site E. White circle indicates the analysed grain.

Figure 6: Time-series of P concentration and Fe-P ratios in SPM at sites A, B and E under baseflow

conditions between May 2012 and March 2014. The smooth lines are 15 point, second order Savitzky-

Golay filters.

587 **Figure 7:** Ratios of oxalate vs. dithionate extractable Al and Fe in baseflow SPM at sites A, B and E

588 between May 2012 and March 2014. The smooth black line is a 15 point, second order Savitzky-

589 Golay filter.

Tables

Table 1: Selected geochemistry data for SPM and source area sediments collected in mini-catchments A, B and E of the River Blackwater. μ is the mean, σ is the standard deviation.

SPM/ Source Area	Statistic	Concentrations (weight %)								Fe:P Ratio	Fe:POC Ratio	Al$_{ox}$: Al$_{di}$ Ratio	Fe$_{ox}$: Fe$_{di}$ Ratio
		Al	Ca	Ce*	Fe	Mg	Mn	P	POC				
Baseflow SPM	μ	7.77	17.34	55	7.56	0.65	0.11	0.35	12.35	22.91	0.64	0.79	0.16
(*n* = 222)	σ	1.31	3.91	6	1.62	0.12	0.03	0.13	2.13	5.58	0.20	0.41	0.15
Storm Event SPM	μ	8.29	14.24	60	6.87	0.66	0.13	0.32	13.78	23.44	0.52	0.62	0.15
(*n* = 721)	σ	1.99	4.16	9	0.98	0.13	0.04	0.11	2.97	6.57	0.13	0.69	0.09
Channel Banks	μ	6.63	33.92	37	4.74	0.63	0.02	0.07	2.21	76.33	3.22	0.18	0.43
(*n* = 60)	σ	2.35	9.80	16	1.78	0.19	0.03	0.03	2.01	27.20	1.84	0.25	0.61
Field Drains	μ	6.66	14.25	60	6.88	0.53	0.19	0.27	7.89	33.67	0.98	1.00	0.42
(*n* = 48)	σ	2.96	10.75	28	4.59	0.27	0.26	0.26	3.61	15.04	0.66	0.67	0.78
Road Verges	μ	10.50	4.82	88	5.55	0.91	0.16	0.32	12.96	17.59	0.45	0.44	0.26
(*n* = 60)	σ	1.76	2.13	8	0.90	0.20	0.03	0.04	2.39	3.87	0.12	0.19	0.14
Topsoils	μ	14.23	3.18	94	6.53	0.84	0.12	0.29	10.22	23.90	0.67	0.63	0.25
(*n* = 60)	σ	1.91	3.29	11	0.83	0.11	0.02	0.07	2.30	6.71	0.17	0.14	0.16

*Ce concentration in ppm

Table 2: Baseflow multiple linear regression model results for the prediction of log-P at sites A (n = 74), B (n = 74) and E (n = 74) between May 2012 and March 2014. VIF is the variance inflation factor; VE is the variance explained; CV is the independent 10-fold cross-validation.

Site A	Predictor	Estimate	Std. Error	t-value	p-value	VIF	Proportion of VE (R^2)
	Fe	0.147	0.010	15.29	<0.001	1.03	0.370
	Ti	-3.865	0.418	-9.24	<0.001	3.47	0.224
	Al_{ox}	1.357	0.310	4.37	<0.001	2.34	0.156
	POC	0.058	0.009	6.16	<0.001	1.15	0.078
	Mg	1.160	0.196	5.92	<0.001	2.47	0.048
	Al_{di}	-1.062	0.275	-3.86	<0.001	1.50	0.020
						Total R^2	0.895
						CV R^2	0.850

Site B	Predictor	Estimate	Std. Error	t-value	p-value	VIF	Proportion of VE (R^2)
	Si	0.023	0.002	12.84	<0.001	1.45	0.445
	Fe	0.115	0.018	6.34	<0.001	3.64	0.123
	POC	0.017	0.005	3.36	<0.001	1.95	0.078
	Ce	-92.764	16.291	-5.69	<0.001	2.20	0.062
	Mn	0.955	0.268	3.57	<0.001	1.60	0.049
						Total R^2	0.757
						CV R^2	0.716

Site E	Predictor	Estimate	Std. Error	t-value	p-value	VIF	Proportion of VE (R^2)
	Ti	-4.090	0.219	-18.69	<0.001	3.76	0.449
	Fe	0.131	0.008	17.39	<0.001	1.70	0.382
	Mg	0.880	0.181	4.86	<0.001	5.43	0.112
	POC	0.027	0.006	4.47	<0.001	1.62	0.014
						Total R^2	0.957
						CV R^2	0.950

Table 3: Storm event multiple linear regression model results for the prediction of log-P in SPM at sites A ($n = 254$), B ($n = 251$) and E ($n = 216$) between May 2012 and March 2014. VIF is the variance inflation factor; VE is the variance explained; CV is the independent 10-fold cross-validation.

Site A	Predictor	Estimate	Std. Error	*t*-value	*p*- value	VIF	Proportion of VE (R^2)
	Mn	2.184	0.259	8.43	<0.001	3.73	0.275
	POC	0.042	0.003	13.65	<0.001	2.56	0.212
	Stage	-0.281	0.035	-8.01	<0.001	2.65	0.182
	Fe	0.117	0.010	11.55	<0.001	3.25	0.101
	K	0.557	0.062	8.95	<0.001	7.59	0.078
	Ti	-2.360	0.201	-11.76	<0.001	6.99	0.043
	Al_{di}	-0.844	0.094	-8.96	<0.001	2.01	0.031
	Fe_{di}	-0.046	0.007	-6.74	<0.001	1.38	0.013
						Total R^2	0.936
						CV R^2	0.927

Site B	Predictor	Estimate	Std. Error	*t*-value	*p*- value	VIF	Proportion of VE (R^2)
	POC	0.074	0.003	24.53	<0.001	1.44	0.619
	Si	0.014	0.001	8.35	<0.001	1.19	0.038
	Fe_{di}	-0.076	0.009	-8.49	<0.001	1.99	0.037
	Al	0.021	0.003	6.62	<0.001	1.79	0.019
						Total R^2	0.714
						CV R^2	0.701

Site E	Predictor	Estimate	Std. Error	*t*-value	*p*- value	VIF	Proportion of VE (R^2)
	POC	0.052	0.003	17.48	<0.001	1.68	0.200
	Si	0.019	0.002	9.84	<0.001	4.06	0.174
	Mn	1.527	0.255	6.00	<0.001	1.88	0.165
	Ti	-2.123	0.251	-8.45	<0.001	9.84	0.150
	Al_{di}	-0.957	0.078	-12.30	<0.001	1.44	0.130
	Fe	0.136	0.010	13.35	<0.001	1.91	0.055
	Mg	0.619	0.135	4.60	<0.001	5.39	0.035
	Fe_{di}	-0.055	0.009	-6.13	<0.001	1.68	0.031
						Total R^2	0.940
						CV R^2	0.932

Figure 1: The Blackwater sub-catchment study area, showing land cover types in mini-catchments A, B and E, with the wider River Wensum catchment also shown
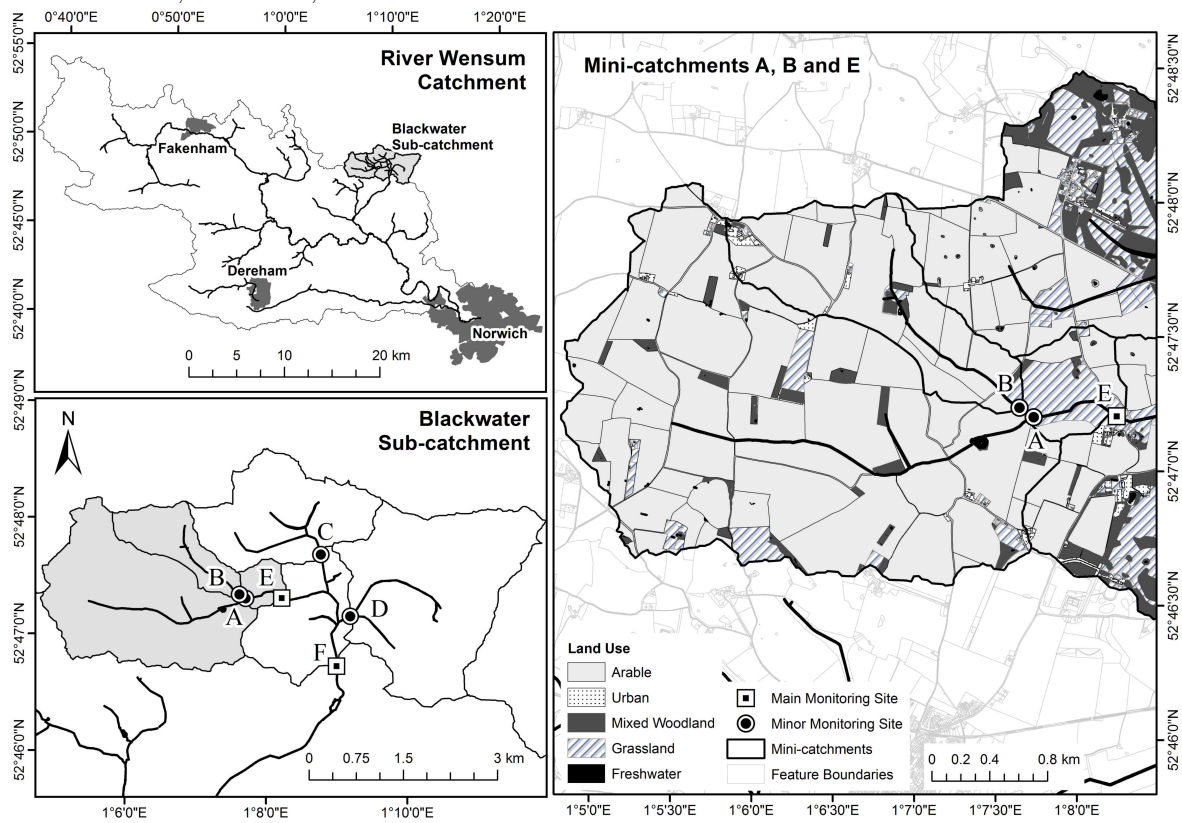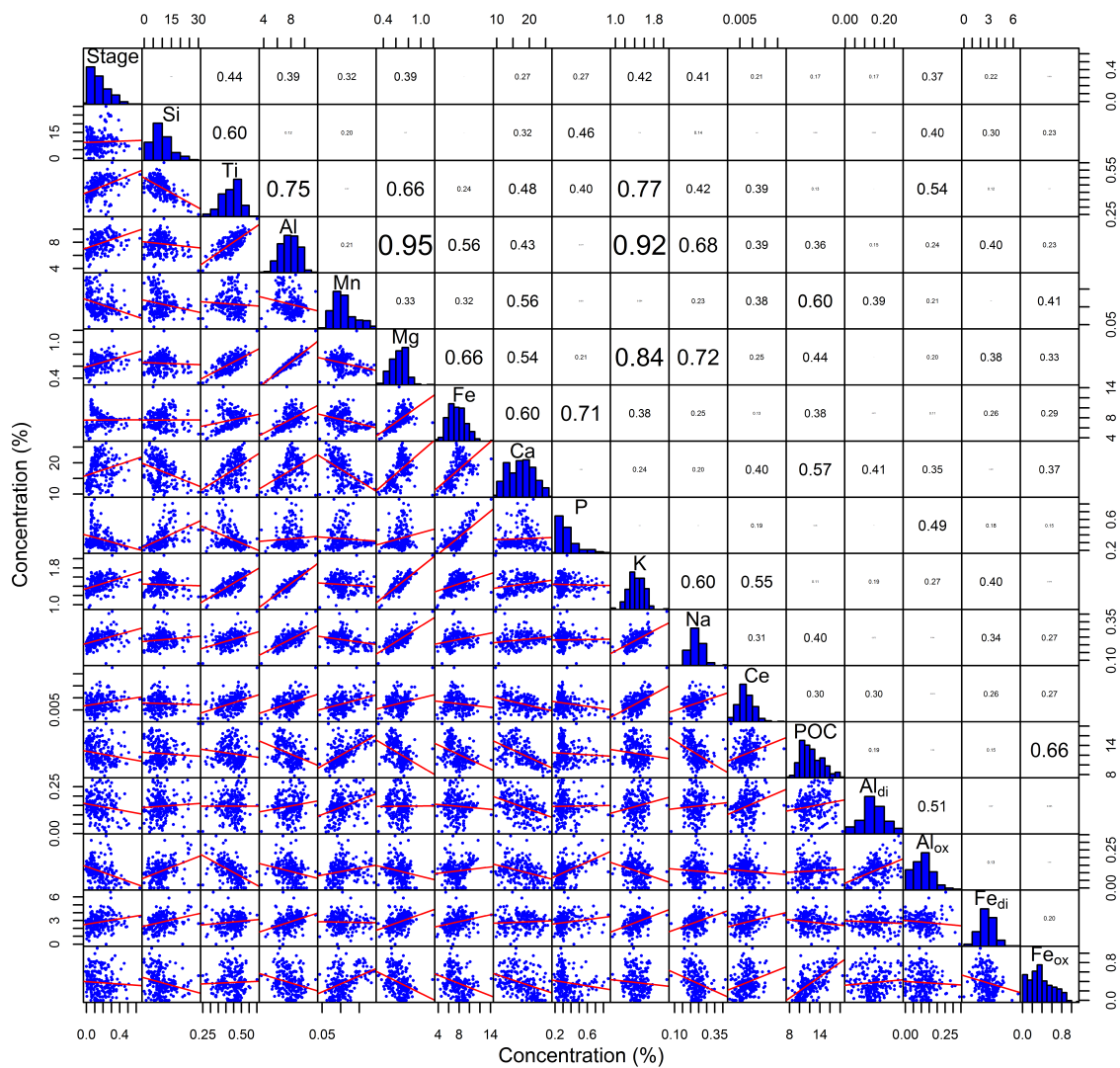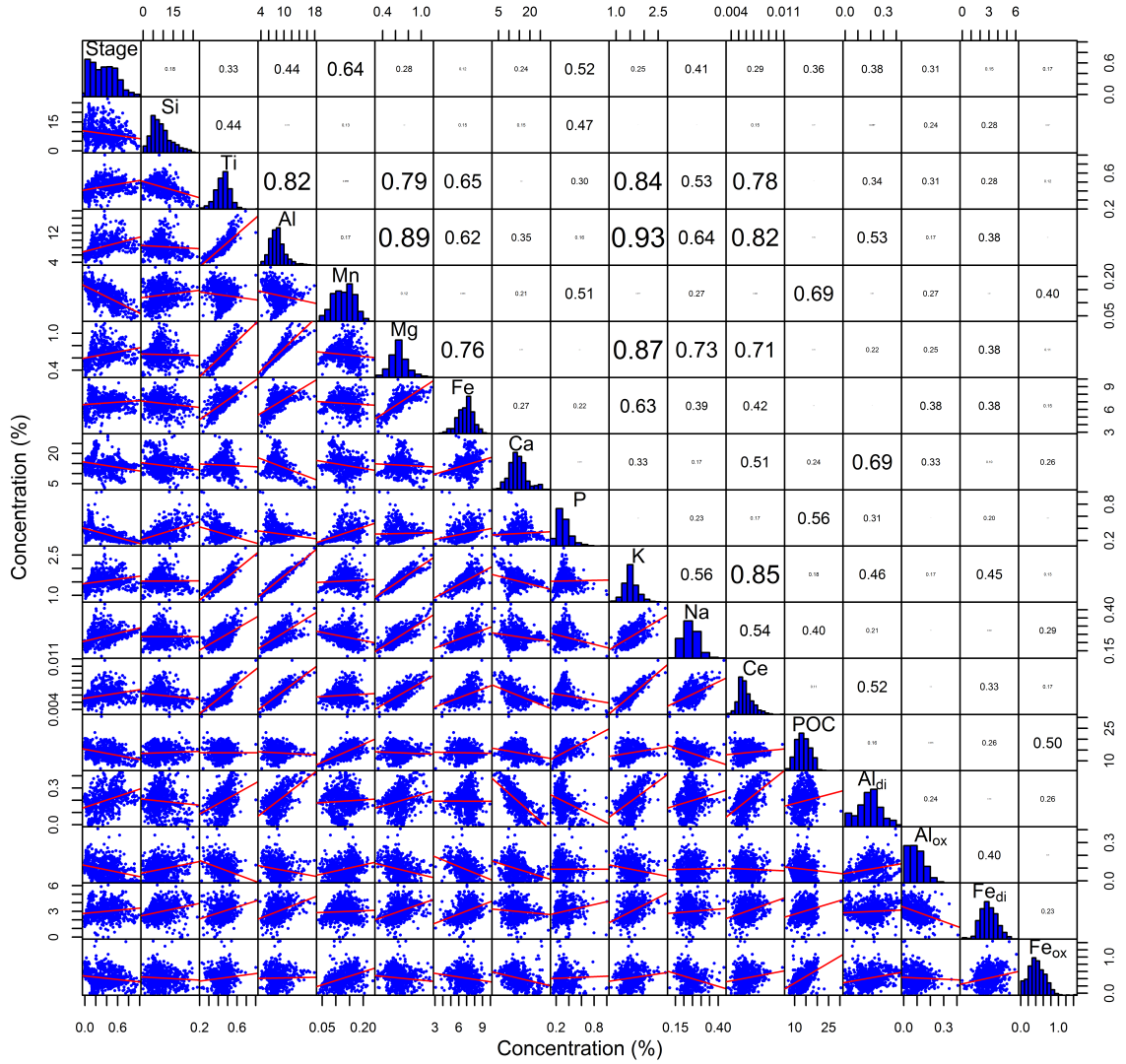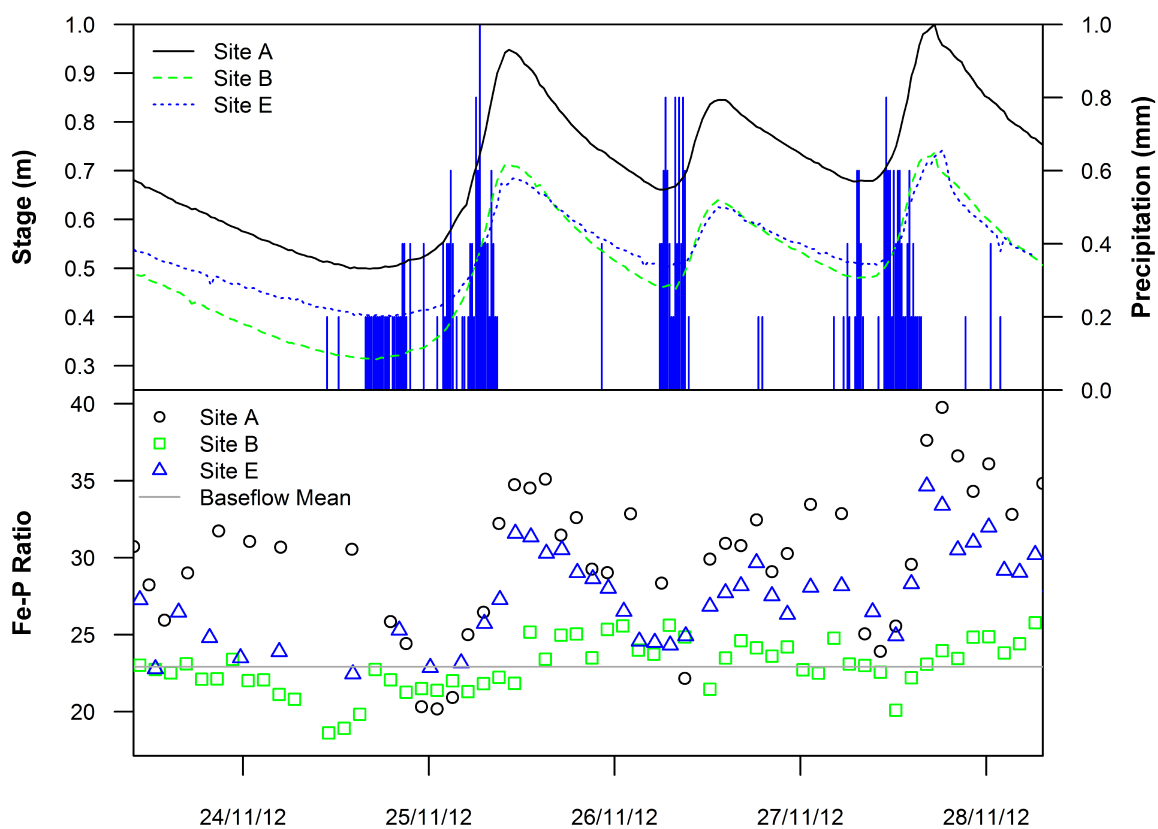
Figure 2: Correlation panel plot of SPM geochemistry (%by weight) under baseflow conditions at sites A, B and E (n = 222). Stage is recorded in meters. The upper right section displays Pearsons correlation coefficients with the text size proportional to correlation strength. The bottom left panel shows the SPM samples (points) and linear regression (line). Central histograms show the distribution of values for each parameter.

. 2.pdf

Figure 3: Correlation panel plot of SPM geochemistry (% by weight) under storm event conditions at sites A, B and E (n = 721). Stage is recorded in meters. The upper right section displays Pearsons correlation coefficients with the text size proportional to correlation strength. The bottom left panel shows the SPM samples (points) and linear regression (line). Central histograms show the distribution of values for each parameter.

.

3.pdf

Figure 4: Time-series of SPM Fe;P ratios for sites A, B and E during three consecutive storm events in November 2012. Baseflow mean refers to the average for all three sites.

4.pdf

Figure 5: Evidence of iron sulphides revealed by an SEM-EDS analysis of sediment collected from the streambed surface (0-6 cm depth) at site E. White circle indicates the analysed grain.
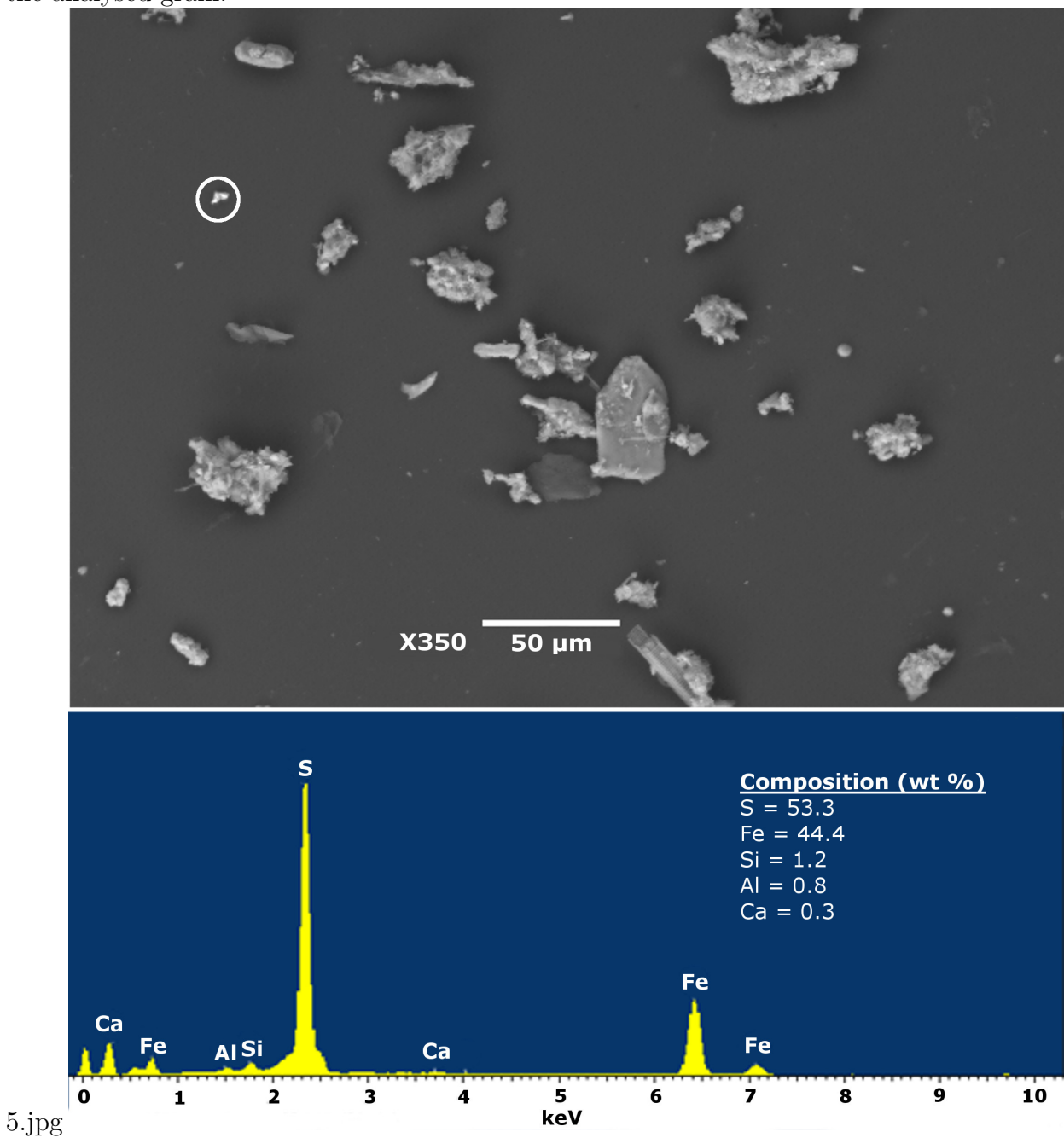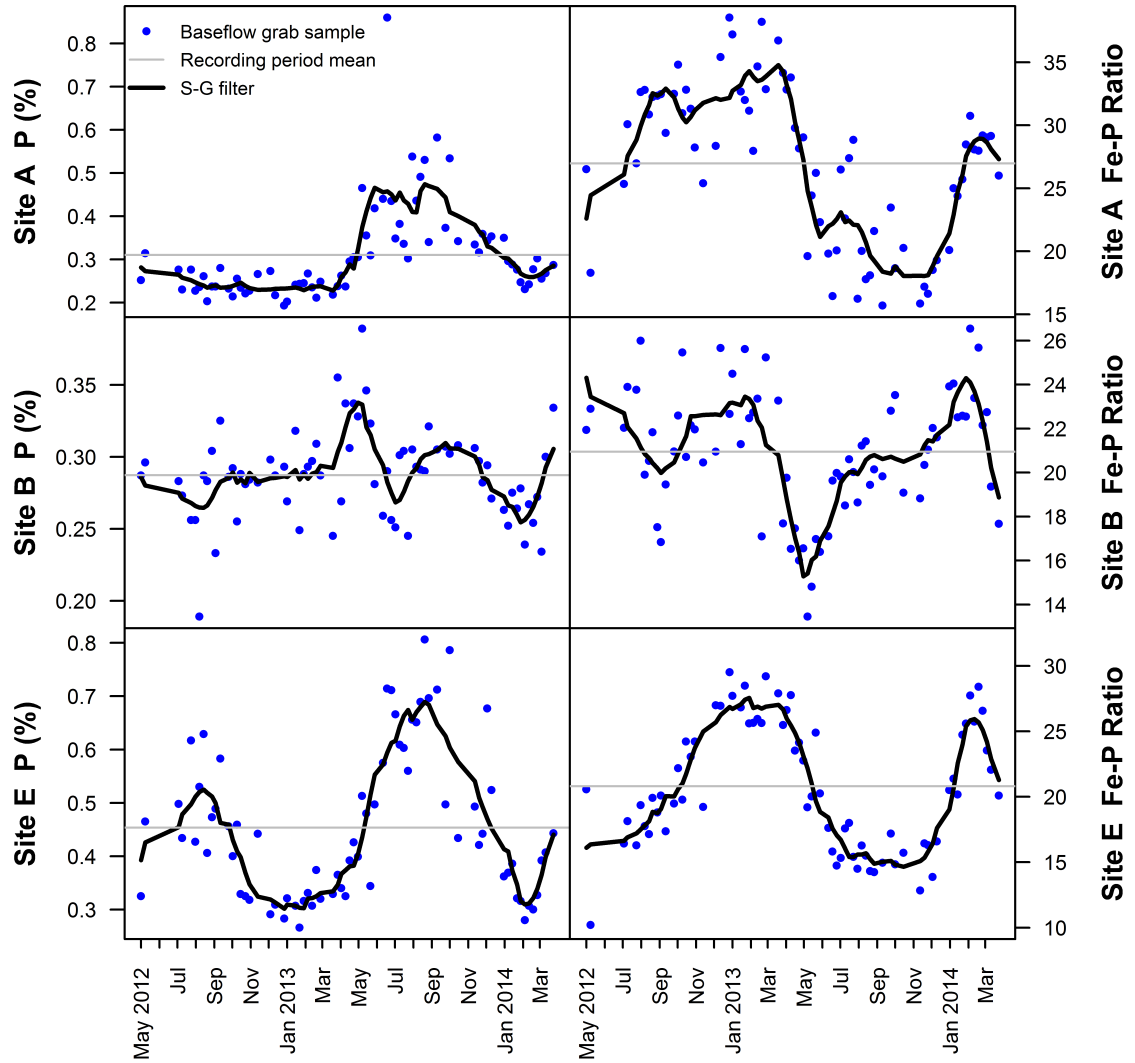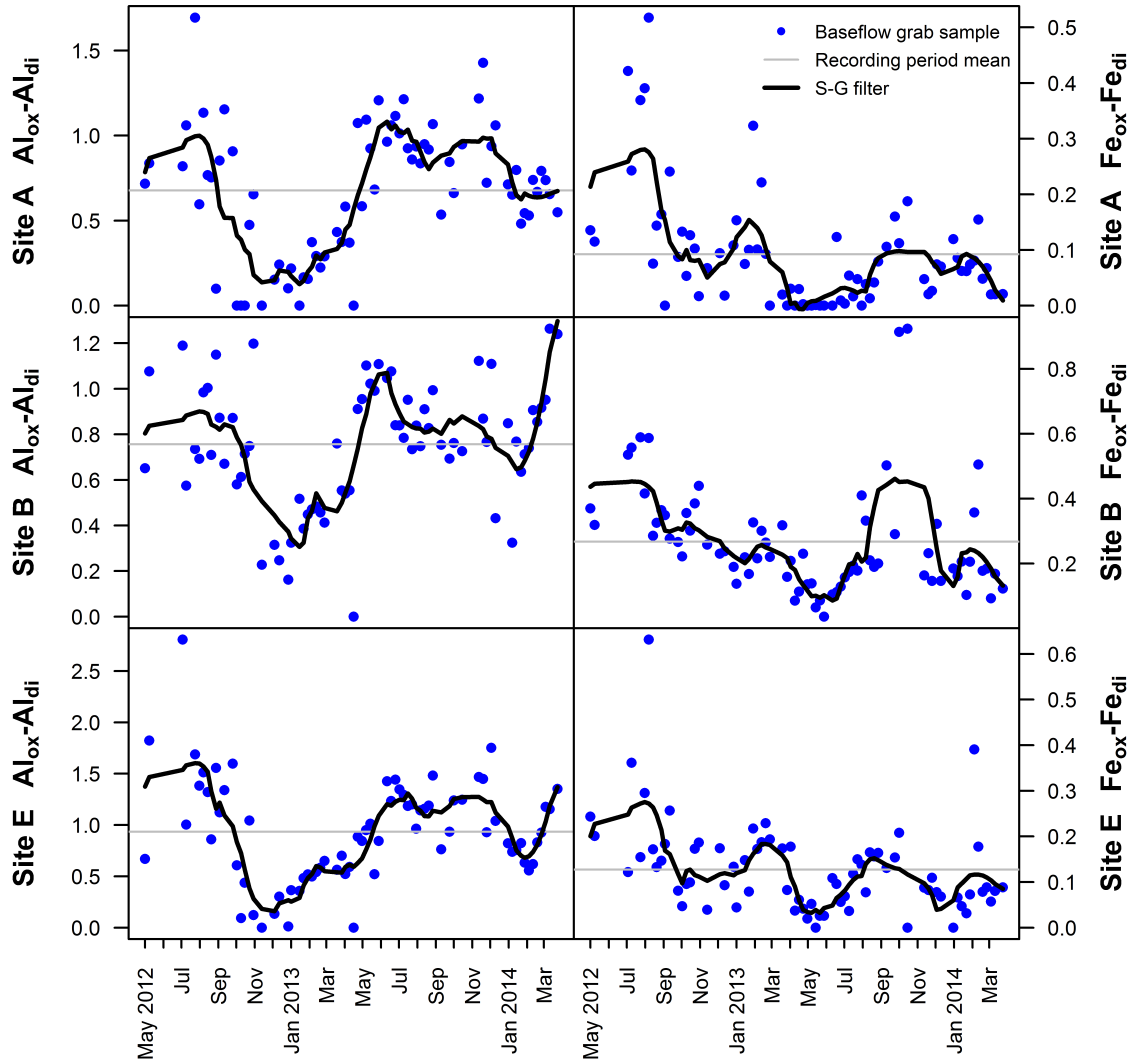
Figure 6: Time-series of P concentration and Fe-P ratios in SPM at sites A, B and E under baseflow conditions between May 2012 and March 2014. The smooth lines are 15 point, second order Savitzky-Golay filters.

6.pdf

Figure 7: Ratios of oxalate vs. dithionate extractable Al and Fe in baseflow SPM at sites A, B and E between May 2012 and March 2014. The smooth black line is a 15 point, second order Savitzky-Golay filter.

7.pdf